Batteries & Supercaps

Research Article
doi.org/10.1002/batt.202500357

Chemistry Europe
European Chemical Societies Publishing

www.batteries-supercaps.org

Impact of Graphene Oxide Lateral Size on the Long-Term Stability of $LiNi_{0.5}Mn_{1.5}O_4$ Electrodes

Marie Uth, Jannie K. Verdelin, Kristian B. Buhl,* Johan Hjelm, Steen U. Pedersen, Kim Daasbjerg,* and Dorthe B. Ravnsbæk*

Increasing the operating voltage of Li-ion batteries is crucial for enhancing the energy density. However, high-voltage batteries suffer from long-term stability issues. Graphene materials used as electrode additives have previously been shown to improve performance, yet the impact of variations in the graphene materials has not been thoroughly explored. Herein, we explore the effect of graphene oxide (GO) drop-in additives with different lateral sizes in $LiNi_{0.5}Mn_{1.5}O_4$ (LNMO)-positive electrodes. The additive reduces polarization of the LNMO electrode under long-term cycling, leading to stability improvements, with the smaller lateral size proving to be superior.

1. Introduction

Spinel $LiNi_{0.5}Mn_{1.5}O_4$ (LNMO) is a cobalt-free, water-compatible electrode material for Li-ion batteries operating at a working potential of 4.7 V versus Li/Li^+.[1,2] While its high operating voltage contributes to a high energy density, it also introduces stability issues. Current electrolyte systems typically consist of organic carbonates and Li salts, such as $LiPF_6$, which degrade over time at high potentials, particularly on the surface of carbon black additives used to enhance electronic conductivity in the electrode.[3–5] This degradation produces hydrofluoric acid (HF), which can erode the surface of metal oxides such as LNMO. Over the past decade, numerous strategies have been explored to address this issue, including coating LNMO with aluminum phosphate,[6] aluminum oxide,[7] titanium oxide,[8,9] soft carbon,[10,11] and, to a large extent, graphene and graphene oxide (GO) materials.[12–22] All of these strategies have demonstrated performance improvements for LNMO. Graphene materials encompass a vast parameter space, where not only the lateral size and number of layers can vary, but also the degree of oxidation and the type of defects in the carbon lattice and heteroatoms or charged species can be tailored into the structure. These variations have a significant impact on the physical properties of graphene, including electrical conductivity, polarity, and mechanical strength. Therefore, it is essential to consider these differences when comparing experimental results.

Table 1 summarizes previous studies on LNMO electrodes incorporating graphene, GO, or reduced GO (rGO). This work employs the term "graphene materials" as a general term encompassing graphene, GO, rGO, and their variants with and without heteroatom doping. The studies report a wide range of optimal graphene material content, varying from 0.5 to 16 wt%. This variation may arise from differences in the types of graphene materials used, as well as the lack of standardized graphene characterization. Key parameters such as lateral size, oxygen content, and the number of graphene layers are often omitted from these studies, making it difficult to compare and replicate results and advance research in the field.

Several studies have reported decreased impedance and electrical and ionic resistance in electrodes containing graphene materials, indicating improved carbon-binder domains with enhanced electrical pathways and electrolyte diffusion. A stable carbon-binder domain is crucial for current distribution in the electrode, as LNMO itself has inherently low electrical conductivity (2.4×10^{-6} S cm^{-1}).[23] Graphene additives in $LiNi_{0.8}Mn_{0.1}Co_{0.1}O_2$ (NMC811) electrodes have been shown to alter the pore size from 0.1 to 2 μm.[24] This enhances Li-ion mass transport in the electrode and diffusion coefficients, as demonstrated by the galvanostatic intermittent titration technique

M. Uth, S. U. Pedersen, K. Daasbjerg
The Novo Nordisk Foundation CO2 Research Center
Department of Chemistry
Aarhus University
Gustav Wieds Vej 10C, Aarhus C 8000, Denmark
E-mail: kdaa@chem.au.dk

M. Uth, D. B. Ravnsbæk
Center for Sustainable Energy Materials
Department of Chemistry
Aarhus University
Langelandsgade 140, Aarhus C 8000, Denmark
E-mail: dorthe@chem.au.dk

M. Uth, J. K. Verdelin, K. B. Buhl
Danish Graphene ApS
Tysklandsvej 7, Vejle 7100, Denmark
E-mail: kbb@danishgraphene.com

J. Hjelm
Department of Energy Conversion and Storage
Technical University of Denmark
Fysikvej 310, Kgs Lyngby 2800, Denmark

Supporting information for this article is available on the WWW under https://doi.org/10.1002/batt.202500357

Table 1. Overview of studies with graphene materials used in LNMO electrodes.

Graphene material	Size	Content	Application method[a)]	Capacity retention[b)]	Suggested mechanism	Ref.
GO, Graphene Supermarket	Lateral: 5 µm, thickness: 8 nm	2.5 wt%	Ultrasonication (US) and coprecipitation in ethanol	89.1% after 200 cycles at 3 C	Conductive network and suppression of CEI	[12]
GO, Hummers method	NA	4.7 wt%	Stirring in ethanol. Annealed at 90 °C	61% after 1000 cycles at 0.5 C	Decreased impedance	[13]
Partially reduced GO, NanoInnova	Thickness: 0.7–1.2 nm	NA	Stirring in ethanol. Dried at 45 °C	90% after 100 cycles at 1 C	CEI suppression	[14]
rGO, NanoInnova	NA	NA	Dry mixing	92% after 100 cycles at 1 C	Improved electrical conductivity and CEI suppression	[15]
GO, Hummers method	NA	16 wt%	Stirring and US in ethanol. Calcination at 400 °C	94% after 280 cycles at 1 C	Suppression of side reactions	[16]
Graphene sheets	NA	2.5 wt%	In situ growth from poly(methyl methacrylate) with $FeSO_4$ catalyst at 650 °C	98.5% after 100 cycles at 0.1 C	Improved electronic and ion-conducting paths, and buffering volume expansion/contraction	[17]
p-Phenylene diamine rGO from GO	Lateral: >100 nm	20 µg cm^2	Electrophoretic deposition of GO films on finished electrodes	81.7% after 1000 cycles at 1 C	Stabilized CEI layer by hindering the formation of F radicals	[18]
GO, Hummers method	NA	0.5 wt%	LNMO pretreatment with poly (allylaminehydrochlorine), US and stirring in GO solution, and annealing at 400 °C	82.5% after 1000 cycles at 20 C	Corrosion protection	[19]
GO, Hummers method	NA	0.5 wt%	LNMO pretreatment with chitosan, US in GO suspension and hydrothermally reacted at 180 °C	96.5 mAh g^{-1} after 1000 cycles at 20 C	Reduction in polarization and charge transfer resistance. Suppression of transition metal dissolution and side reactions. Extended solid-solution reaction and less volume change	[20]
Sulfonated graphene, Suzhou Qualcomm New Materials Tech. Co., Ltd.	NA	2 wt%	Mixing and rotary evaporation	97.6% after 1000 cycles at 1 C	CEI suppression, reduced polarization, and charge transfer resistance. Suppression of transition-metal dissolution and side reactions. Enhanced diffusion kinetics	[21]

[a)]The graphene material was in all cases applied as a pretreatment to the LNMO before electrode slurry preparation. [b)]Highest capacity retention from each study is presented.

(GITT) and electrochemical impedance spectroscopy (EIS) measurements.[24]

In addition, the cited literature often uses lab-grown LNMO particles, which can vary in quality and size, potentially leading to inconsistent performance in reference systems. As a result, their findings may differ significantly from those obtained with commercial-grade systems. To ensure a more robust and practical benchmark, this study employs commercially available LNMO from Topsoe, providing greater relevance for battery applications.

This study demonstrates the impact of incorporating an electrochemically oxidized type of few-layered GO as an additive in LNMO electrodes. Electrochemically oxidized graphene holds greater industrial relevance than chemically oxidized graphene due to its environmentally friendly, low-waste production methods, which contribute to cost reductions.[25,26] We explore the effect of two different flake sizes in a mass fraction range from 0.05 to 0.5 wt% as a drop-in additive to the electrode slurry. The method demonstrated here is highly applicable in industrial settings, as it requires no pretreatment of the LNMO. The GO additive is simply introduced into the electrode slurry during an already established mixing step, ensuring seamless integration into existing manufacturing processes.

2. Results and Discussion

Two commercially available few-layered GO samples were characterized in terms of lateral flake size, oxygen content, and characteristic Raman signals: D (1340 cm^{-1}), G (1570 cm^{-1}), and 2D (2670 cm^{-1}). The intensity ratio I_D/I_G and the full width at half maximum of the 2D peak ($I_{2D,\ FWHM}$) serve as indicators of the defect degree.[27] The results are presented in **Table 2**.

The sample of small GO flakes (i.e., **GS**) had an average size of 0.9 ± 0.4 µm measured by scanning electron microscope (SEM)

Research Article
doi.org/10.1002/batt.202500357
Chemistry Europe
European Chemical Societies Publishing

Table 2. Overview of the GO samples used in this work.

Sample name[a)]	Lateral size [μm]	Thickness [nm]	I_D/I_G	$I_{2D,\ FWHM}$ [cm^{-1}]	O [at%]
GS	0.9 ± 0.4	3.6 ± 1.0	1.16	89.7	12.7 ± 0.6
GM	5 ± 2	3.5 ± 0.8	1.18	88.5	17.4 ± 0.2

[a)]Sample names are denoted "G" for "graphene oxide" and "S" or "M" for "small" or "medium", respectively.

and 13 at% oxygen measured by SEM-energy-dispersive X-ray spectroscopy (EDX). The medium-sized GO flakes (i.e., **GM**) were, on average, 5 ± 2 μm measured from optical microscopy and had 17 at% oxygen. The remaining atoms were carbon in both cases. Although both samples underwent the same oxidation process during production, the **GS** sample was partially reduced during processing to achieve a smaller lateral size (as reported by the manufacturer). The Raman spectra of bulk **GS** and **GM** (Figure S2, Supporting Information) are highly similar, indicating that the defect degree in the carbon lattice is comparable between the two samples. The primary difference between the samples is the flake size. Therefore, this parameter is the focus of this study.

Table 3. Specifications of electrodes.

Sample name[a)]	GO in electrode [wt%]	Average capacity loading [mAh cm^2][b)]	ε [%][c)]
Blank	0	1.2	30
$\mathbf{GS_{0.05}}$	0.05	1.2	28
$\mathbf{GS_{0.10}}$	0.10	1.5	31
$\mathbf{GS_{0.25}}$	0.25	1.3	34
$\mathbf{GS_{0.50}}$	0.50	1.2	29
$\mathbf{GM_{0.05}}$	0.05	1.3	30
$\mathbf{GM_{0.10}}$	0.10	1.4	14
$\mathbf{GM_{0.25}}$	0.25	1.3	23
$\mathbf{GM_{0.50}}$	0.50	1.3	21

[a)]Letter code refers to GO type (see Table 2) and subscript denotes the GO weight fraction of the electrode dry matter content. [b)]Average capacities are theoretical values based on the theoretical capacity of LNMO at 147 mAh g^{-1}. [c)]The porosity, ε, is a theoretical measure calculated based on the length, thickness, and weight of the electrodes, as well as the densities (as informed by the suppliers) of the materials.

Electrodes without graphene, composed of LNMO/SuperC65/PVDF in a 92:4:4 ratio, were prepared to serve as a baseline for evaluating the impact of GO additives. These electrodes are referred to as the "blank" in the following text. For the GO-containing electrodes, a paste with 2 wt% GO in NMP was incorporated as a simple drop-in additive to the electrode slurry. The GO content in the electrodes varied from 0.05 to 0.5 wt% of the total dry matter and replaced a fraction of the superC65, making the combined dry matter of GO and superC65 4 wt% of the total dry matter. The theoretical average capacities and theoretical porosities (ε) for each electrode cast are presented in **Table 3**.

SEM was used to investigate the spatial distribution of GO in the electrode (**Figure 1**). The LNMO polycrystals are observed as multiparticle spheres with diameters ranging from 4 to 8 μm. In the blank electrode (Figure 1a), the SuperC65 particles, which are small spheres only a few nanometers in size, appear as a darker, more porous structure compared to LNMO. The binder is not distinctly visible but is expected to be primarily associated with the SuperC65, helping to adhere the conductive carbon to the active material and the current collector in what is known as the carbon-binder domain.

The SEM images of electrodes containing GO additives (Figure 1b,c) reveal GO as contours surrounding the LNMO particles and within the carbon-binder domain. GO encapsulates some LNMO particles and forms bridges between them. No visible morphological changes are observed in the carbon-binder domain when using **GS** and **GM** additives at concentrations of 0.5 wt% and below. Additional SEM images are available in Figure S10–S15, Supporting Information.

The studies reviewed in Table 1 utilize different types of graphene material and LNMO particle sizes, which significantly affect the electrode morphology. However, they also pursue distinct objectives with the use of graphene materials. References

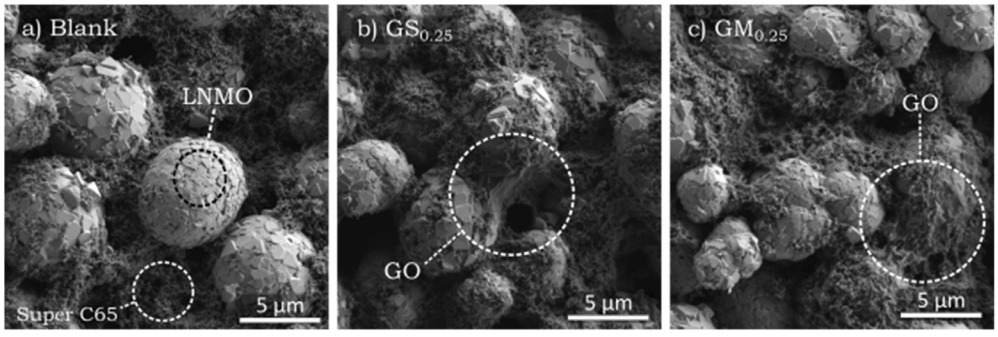

Figure 1. SEM images obtained from as-prepared a) LNMO electrode (blank), b) $\mathbf{GS_{0.25}}$, and c) $\mathbf{GM_{0.25}}$.

Research Article
doi.org/10.1002/batt.202500357
Chemistry Europe
European Chemical Societies Publishing

13–16, 18, and 20 focus on coating the LNMO to suppress corrosion of the active material, while references 12, 17, 19, and 21 aim to leverage the conductive properties of graphene materials without emphasizing encapsulation of the LNMO particles. Despite these differing goals, the use of graphene materials consistently results in increased capacity retention, improved high-rate capacity, and reduced impedance. Encapsulation of LNMO particles does not appear essential for achieving the benefits of graphene materials.

The performance of the electrodes was evaluated using galvanostatic cycling between 3.5 and 5 V. The program included a rate test with discharge current rates of 1, 3, and 5 C (**Figure 2**a,b). The specific discharge capacities at 1 and 3 C are higher for **GS** than for **GM** electrodes, while both types outperform the blank electrode. At 5 C, the capacity for the $\mathbf{GS}_{0.1}$ drops to 132 mAh g^{-1}, which is lower than for $\mathbf{GS}_{0.5}$, $\mathbf{GS}_{0.25}$, and $\mathbf{GS}_{0.05}$, which all maintain capacities of 134–135 mAh g^{-1}. This decrease correlates with the higher capacity loading of $\mathbf{GS}_{0.1}$ (Table 3, Figure S19, Supporting Information), suggesting that limited mass transport could be responsible for the observed effect. For $\mathbf{GM}_{0.25}$, $\mathbf{GM}_{0.1}$, and $\mathbf{GM}_{0.05}$, the capacity at 5 C drops to 132 mAh g^{-1}, whereas for $\mathbf{GM}_{0.5}$ and the blank sample, the capacity falls below 130 mAh g^{-1}. After the high-rate test, a cycle at 0.1 C confirms full retention of the initial capacity for both the blank and GO-containing electrodes.

The cells were further tested over 49 cycles at a charge rate of 0.5 C and a discharge rate of 1 C, followed by a recovery cycle at 0.1 C, repeated twice. The GO-containing cells exhibit higher capacity than the blank sample, with the **GS** additive outperforming the **GM** additive. Figure 2c shows that the **GS** additive improves the 1 C capacity retention from 98.5% in the blank sample to 98.8%–99.0% in the **GS**-containing samples. As seen from Table 1, 1 C capacity retention of this order of magnitude has not previously been reported. Postmortem SEM analysis of the electrodes (see Supporting Information) showed that the GO stay well dispersed throughout the electrodes after 100 cycles.

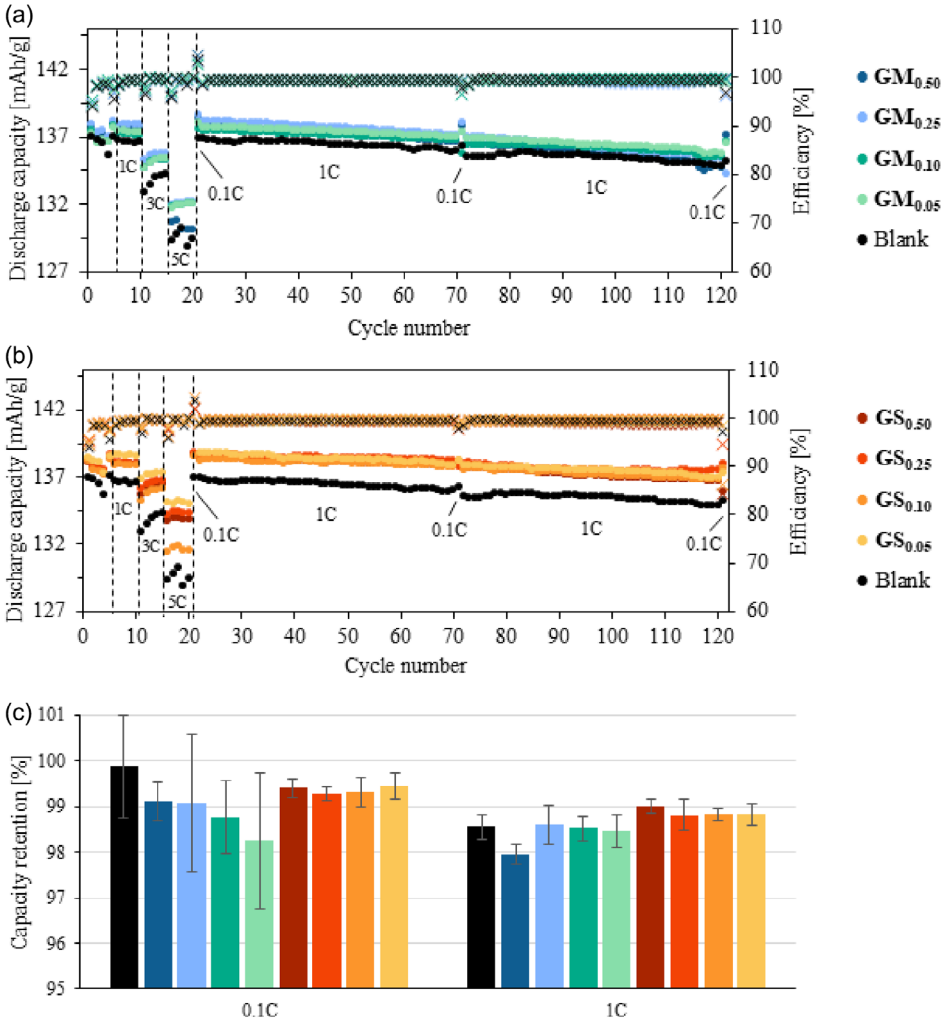

Figure 2. Discharge capacities from galvanostatic cycling of half-cells, including four formation cycles, a max capacity test, rate test of 1, 3, and 5 C discharge rate, 0.1 C for cycles 21, 72, and 123, and continuous cycling at 0.5 C charge and 1 C discharge in cycles 22–71 and 73–122 for a) **GM**- and b) **GS**-containing electrodes. c) Average capacity retention for 3–5 cells with each GO concentration and blank over 100 cycles at 0.5 C charge and 1 C discharge. A cycle at 0.1 C was run before and after achieving the 0.1 C capacity retention, and the first and last cycles at 1 C discharge were used to calculate the 1 C capacity retention.

Research Article
doi.org/10.1002/batt.202500357
Chemistry Europe
European Chemical Societies Publishing

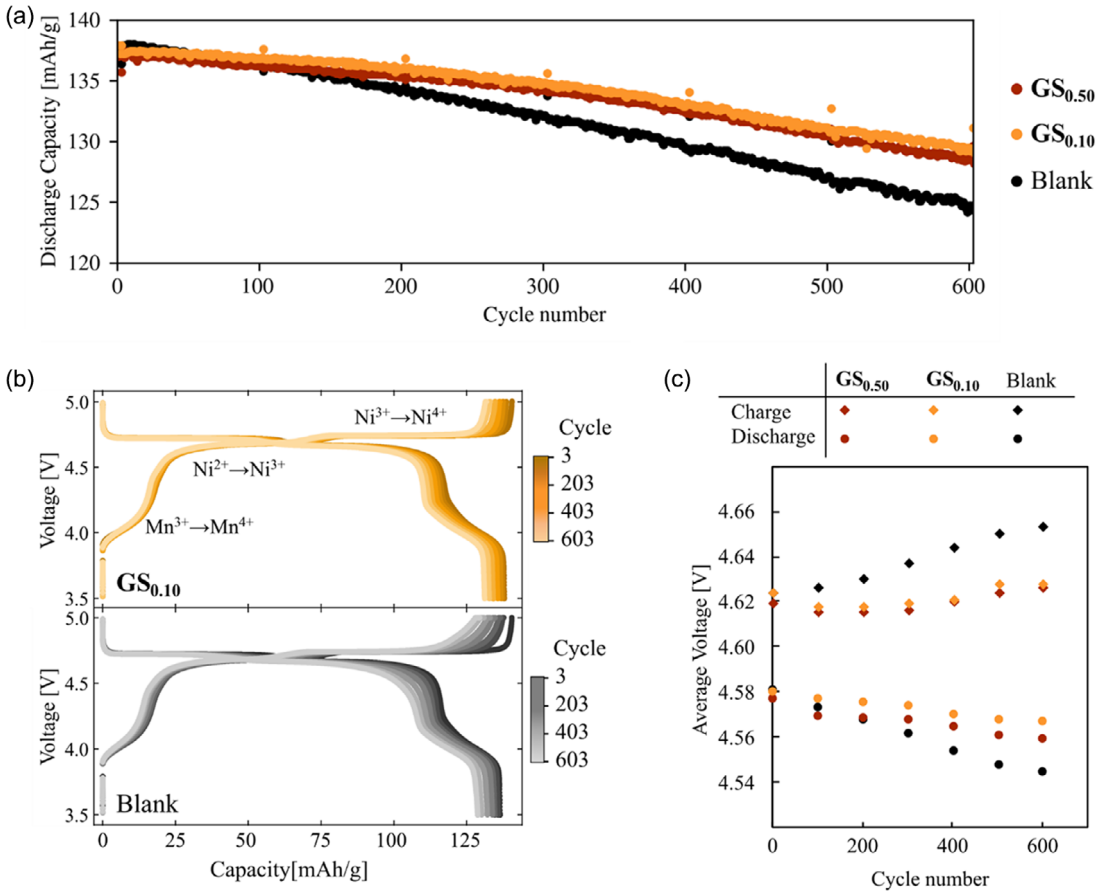

Figure 3. a) Discharge capacities from long-term galvanostatic cycling, including three formation cycles at 0.1 C, followed by repetitive 99 cycles at 0.5 C charge and 1 C discharge and a recovery cycle at 0.1 C. b) Potential profiles of the cycles at 0.1 C for a **$GS_{0.1}$** cell and blank cell. c) Average voltage for charge (diamonds) and discharge (circles) for the cycles at 0.1 C.

As the **GS** additive performed better than the **GM** additive, long-term stability tests were performed for **$GS_{0.1}$** and **$GS_{0.5}$** (**Figure3**a). These show significantly higher long-term capacity retention for the GO-containing cells as compared to the blank one, i.e., after 600 cycles, the capacity retention is 90.2%, 94.1%, and 93.4% at 1 C and 94.4%, 95.1%, and 95.6% at 0.1 C for the blank, **$GS_{0.1}$**, and **$GS_{0.5}$** electrodes, respectively.

The voltage profiles during the 0.1 C cycles for both the blank and GO-containing electrodes initially exhibit nearly identical features (Figure 3b) with a plateau at 4 V corresponding to the Mn^{3+} to Mn^{4+} transition and two plateaus around 4.7 V associated with the Ni^{2+} to Ni^{3+} and the Ni^{3+} to Ni^{4+} transitions. With cycling, the charging potential for the blank sample increases, especially nearing the end of the Ni^{3+} to Ni^{4+} transition plateau. This increased polarization is either caused by increasing kinetic limitations, e.g., a thicker cathode electrolyte interface (CEI) layer or degradation of the electrical pathways, which are suppressed in the presence of GO. The difference between the average voltage of charge and discharge after long-term cycling is significantly higher for the blank sample than for the GO-containing samples (Figure 3c). A similar effect was observed when graphene was added to a lithium iron phosphate (LFP) electrode by Fu et al., who interpreted the decreased polarization as a result of improved electronic conductance in the graphene-containing electrode.[28] We note that powder X-ray diffraction (PXRD) (Figure S20, Supporting Information) shows that GO addition does not induce any structural change to LMNO neither in the pristine state nor after 120 cycles.

As seen in the rate test, the electronic conductivity is slightly improved in the GO-containing samples compared to the blank. Since highly oxidized GO is an insulating material,[29,30] the improved electrical conductivity in the electrodes is likely obtained by GO supporting the carbon-binder domain. The much larger increase in the polarization during cycling in the blank electrodes (Figure 3c) further indicates that GO stabilizes the carbon-binder domain and prevents degradation of electronic pathways. This leads to the conclusion that GO preserves the electrical network under long-term cycling by being a structural support for the carbon-binder domain.

EIS measurements (Figure S21, Supporting Information) indicate no significant change in tortuosity with the introduction of GO (Table S2, Supporting Information). This shows that lithium diffusion in the pores is neither blocked nor improved by the GO sheets. This finding was supported by measurements with GITT, where no clear trends in the Li-ion diffusion in the presence/amounts of GO were observed (Figure S22—S32, Supporting Information).

Carbon black is known to catalyze electrolyte degradation, raising concerns that graphene additives, with their large carbon

Research Article
doi.org/10.1002/batt.202500357
Chemistry Europe
European Chemical Societies Publishing

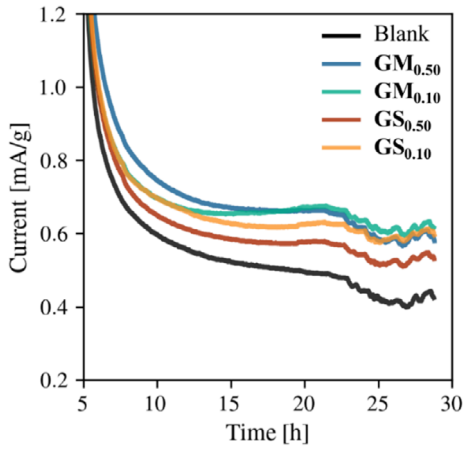

Figure 4. Chronoamperometry of half-cells at 5 V conducted after 6 h resting time, two formation cycles, and a full charge in half-cells. The potential was held at 5 V for 24 h.

surface, may exacerbate electrolyte degradation. To investigate this potential issue, chronoamperometry was performed by keeping the cell at 5 V for 24 h (**Figure 4**). At this voltage, all lithium ions are extracted from the LNMO structure, meaning that the measured residual current must originate from side reactions, such as electrolyte degradation. The results show that GO-containing electrodes indeed exhibit a higher current than the blank. Especially in half-cells, electrolyte degradation can lead to an artificially higher capacity, as these systems contain excess electrolyte and an abundant lithium supply from the reference electrode. However, in commercial full cells, the electrolyte volume is minimized to reduce the battery weight, and the lithium inventory is restricted to the initial content in the positive electrode and the electrolyte.

High-voltage stability of electrolytes remains a widely recognized challenge and is currently the subject of extensive research.[31] We note that in this study, a standard 1 M $LiPF_6$ EC:DEC electrolyte without any stabilizing additives, which may prevent severe electrolyte decomposition, was used. Hence, to fully harness the benefits of GO additives in long-term cycling, further research is needed to evaluate electrolyte stability in GO-containing electrodes within full-cell configurations. Ideally, these studies should be conducted using novel electrolyte systems designed explicitly for high-voltage stability.

3. Conclusion

Testing GO with two different flake sizes in concentrations from 0.05 to 0.5 wt% in the electrodes by direct addition to the electrode slurry showed that the addition of electrochemically oxidized graphene with an average size of 0.9 µm gave the most significant improvement in capacity retention over 100 cycles, i.e., 98.8%–99.0% compared to 98.4% for the blank sample. During galvanostatic cycling over 600 cycles, GO-containing electrodes retained 94.1% and 93.4% of their 1 C capacity, whereas the blank electrode retained only 90.2% and exhibited a significant polarization increase. The observed physical variance in GO additives, particularly flake size, influenced electrode performance, underscoring the importance of fully characterizing graphene material in studies of this nature.

To investigate the underlying cause of these improvements, EIS measurements revealed that the **GS** and **GM** additives induced a slight decrease in the tortuosity of the electrodes compared to the blank sample. Furthermore, chronoamperometry detected increased leakage current in GO-containing electrodes at 5 V, indicating increased electrolyte degradation. As commercial battery systems minimize electrolyte volume to reduce weight, applying GO could lead to faster electrolyte depletion. The promising ability of GO to mitigate polarization over 600 cycles compared to the blank sample should be further explored in systems designed with electrolytes optimized for high-voltage stability in future studies.

The combined results do not give clear evidence that the GO is acting as a protective coating or a conductive additive in the fresh electrodes, as previously suggested in the literature. However, long-term experiments indicate that GO prevents polarization increase by preserving the conductive network. The non-conductive nature of GO means that it must act as a structural support for the carbon-binder domain.

4. Experimental Section

Graphene Characterization

Two graphene oxide (GO) samples were acquired as a paste in *N*-methyl-2-pyrrolidone (NMP) (2 wt%). The sample names were denoted "**GS**" for "GO small lateral size" and "**GM**" for "GO medium lateral size". GO flake size was analyzed by depositing a drop of dilute NMP dispersion of GO on a silicon wafer. The wafer was heated to 160 °C and 10 µL of GO/NMP dispersion was drop cast onto the hot wafer. Medium size flakes (>1 µm) (i.e., **GM**) were analyzed directly by optical microscopy,[32] while small flakes (<1 µm) (i.e., **GS**) were analyzed on a boron-doped silicon wafer using a Tescan Clara SEM with a Everhart–Thornley detector. A total of 200 flakes from each sample were analyzed for statistical evaluation. The length and width of the flakes were measured perpendicularly to each other.

Thickness of the **GS** sample was determined using a Bruker Dimension Edge atomic force microscope equipped with an RTESP-300 probe in tapping mode under ambient pressure. Areas of $5 \times 5\ \mu m^2$ were analyzed in 64 lines at a scan rate of 1 Hz. Gwyddion software[33] was used to analyze the obtained data.

Bulk samples of GO paste were dried in a vacuum oven at 80 °C and analyzed by SEM with an EDX detector to determine the oxygen content. Raman spectra of the dried GO pastes were obtained by a Renishaw InVia Raman microscope equipped with a 150 mW 514 nm laser operating at an intensity of ≈5 mW and using a 100× lens. For each experiment, 100 spectra were acquired using a 1 s acquisition time. Wire 4.3 was used for the analysis. Background elimination was performed before analysis using a polynomial procedure.

Electrode Formulation

The electrode slurry formulation and electrochemical test setup were developed based on the methods described in a white paper

published by Haldor Topsoe ApS.[34] The electrode slurries without graphene comprised polycrystalline LNMO (Topsoe) as active material, super C65 (MTI) as a conductive additive, and poly(vinyl difluoride) (PVDF) (MTI) as a binder in the ratio 92:4:4. The PVDF was dissolved in NMP as an 8 wt% solution beforehand. One slurrie contained 2 g of drymatter giving the masses $m_{(LNMO)} = 1.84$ g, $m_{(Super\ C65)} = 0.080$ g, and $m_{(PVDF,8\%\ in\ NMP)} = 1$ g. All components were mixed in a Thinky Mixer at 2000 rpm for at least 10 min with additional NMP to achieve a slurry with 50%–60% dry matter. The slurry was coated onto
carbon-coated aluminum foil using a doctor blade and then dried at 80 °C for at least 2 h. The electrode sheet was transferred to a vacuum oven and dried at 80 °C under vacuum for at least 12 h. The sheet was calendared to a porosity of ≈30% and punched to circular electrodes with a diameter of 14 mm.

In GO-containing electrodes, GO (2 wt% in NMP, Danish Graphene) replaced a weight fraction of the super C65 (0.05–0.5 wt% of the total electrode dry matter content). All other aspects of the production process remained the same as described above. The electrodes were named $\mathbf{GS_X}$ or $\mathbf{GM_X}$ after the **GS** or **GM** additive, respectively, with X being the concentration of the given additive.

Electrochemical Tests

Electrodes were mounted in CR2032 coin cells within an argon-filled glovebox, where the water and oxygen levels were maintained at <1 ppm. A stainless-steel spacer (Ø = 15.5 mm and height = 0.5 mm) was placed in the bottom case with the positive LNMO electrode (14 mm) on top. A Whatman QMA quartz separator (19 mm) was placed on top of the positive electrode, and 100 µL of electrolyte (1 M $LiPF_6$ in ethylene carbonate (EC):diethyl carbonate (DEC) 1:1 v/v) was dripped onto the separator. A disk of lithium foil (Ø = 15 mm and thickness = 100 µm) was used as the negative electrode and carefully placed on top of the separator to align with the positive electrode. Another spacer (Ø = 15.5 mm and height = 0.5 mm) was placed on top of the lithium disk, followed by a cone spring (Belleville) and the top case. The coin cells were closed under a pressure of 750 psi and left to rest for 6 h before electrochemical testing.

The galvanostatic cycling program comprised two formation cycles, initial capacity tests, a rate test, and a stability test. Charging was done under a constant current (CC)/constant voltage setting with a maximum voltage of 5 V and a cutoff current of 0.2 or 0.05 C (see Table S1, Supporting Information). The discharge was CC until 3.5 V. Three to five cells with electrodes of each GO concentration and blank electrodes were cycled. The long-term stability test comprised three formation cycles at 0.1 C followed by repetitive 99 cycles at 1 C and one cycle at 0.1 C. Three blank cells and four cells with $\mathbf{GS_{0.1}}$ and $\mathbf{GS_{0.5}}$ were tested.

Impedance measurements were performed on a Biologic MPG-2 potentiostat from 200 mHz to 20 kHz with 10 points per decade. Symmetric cells with 0% state of charge (SOC) were tested at open circuit voltage. Half-cells were tested in the same frequency range after the initial resting time of 6 h, at 0% SOC. After a full charging/discharging cycle at a current rate of 0.2 C, the impedance at 50% SOC was measured.

Chronoamperometry measurements were conducted after 6 h resting time, two formation cycles, and a full charge in half-cells. The potential was held at 5 V for 24 h. For the GITT experiment the cells were rested 12 h at OCV and following charged and discharged at 0.1 C in steps of 15 min with 1 h relaxation in between.

PXRD was performed on selected electrodes using a Rigaku Smartlab diffractometer employing Cu Kα1 radiation, cross beam optics, and Bragg Brentano geometry. Data was recorded from 15 to 70° 2θ in steps of 0.01° and 0.25 s X-ray exposure per step. The electrodes were mounted on silicon sample holders. The cycled electrodes were not removed from the spacers, used in the coin cells, to keep the electrode intact.

Acknowledgements

We send our gratitude to Myrian E.A. Arcos, Christian F. Elkjær, and Jonathan Højberg at Topsøe for the opportunity to get training in electrode preparation and coin cell assembly with the LNMO material. We acknowledge the Carlsberg Foundation (grant no.: CF20-0364) and iMAT center for the Tescan Clara SEM. We thank the Innovation Fund Denmark (grant no.: 2050-00011B) for funding the project. D.B.R. thank the the Danish National Research Foundation for funding through the Center of Sustainable Energy Materials (DNRF189).

Conflict of Interest

J.K.Verdelin and K.B.Buhl are employees of Danish Graphene ApS, which supplied the GO materials.

Data Availability Statement

The data that support the findings of this study are available from the corresponding author upon reasonable request.

Keywords: electrochemistry · graphene oxide · lithium ion battery · LNMO

[1] Y. Gao, K. Myrtle, M. Zhang, J. N. Reimers, J. R. Dahn, *Phys. Rev. B* **1996**, *54*, 16670.
[2] T. Ohzuku, S. Takeda, M. Iwanaga, *J. Power Sources* **1999**, *81-82*, 90.
[3] R. Younesi, A. S. Christiansen, R. Scipioni, D.-T. Ngo, S. B. Simonsen, K. Edström, J. Hjelm, P. Norby, *J. Electrochem. Soc.* **2015**, *162*, A1289.
[4] J. Syzdek, M. Marcinek, R. Kostecki, *J. Power Sources* **2014**, *245*, 739.
[5] Y.-H. Liu, W.-C. Chen, C.-H. Hsueh, C.-L. Hsu, *Mater. Today Chem.* **2022**, *25*, 100934.
[6] J. Hur, I. T. Kim, *Bull. Korean Chem. Soc.* **2014**, *35*, 3553.
[7] E. R. Østli, Y. Tesfamhret, S. Wenner, M. J. Lacey, D. Brandell, A. M. Svensson, S. M. Selbach, N. P. Wagner, *ACS Omega* **2021**, *6*, 30644.
[8] X. Hao, B. M. Bartlett, *J. Electrochem. Soc.* **2013**, *160*, A3162.
[9] F. U. Okudur, M. Batuk, J. Hadermann, M. Safari, D. De Sloovere, S. K. Mylavarapu, B. Joos, J. D'Haen, M. K. Van Bael, A. Hardy, *RSC Adv.* **2023**, *13*, 33146.
[10] S. Ghosh, M. Mahapatra, S. Bhowmik, K. K. Garlapati, S. K. Martha, *ACS Appl. Energy Mater.* **2023**, *6*, 9390.
[11] D. J. Ku, J. H. Lee, S. J. Lee, M. Koo, B. J. Lee, *Surf. Coat. Technol.* **2019**, *376*, 25.
[12] S. J. R. Prabakar, Y.-H. Hwang, B. Lee, K.-S. Sohn, M. Pyo, *J. Electrochem. Soc.* **2013**, *160*, A832.
[13] X. Fang, M. Ge, J. Rong, C. Zhou, *J. Mater. Chem. A.* **2013**, *1*, 4083.
[14] S. Monaco, F. De Giorgio, L. Da Col, M. Riché, C. Arbizzani, M. Mastragostino, *J. Power Sources* **2015**, *278*, 733.
[15] C. Arbizzani, L. Da Col, F. De Giorgio, M. Mastragostino, F. Soavi, *J. Electrochem. Soc.* **2015**, *162*, A2174.
[16] G. Jia, C. Jiao, W. Xue, S. Zheng, J. Wang, *Solid State Ionics* **2016**, *292*, 15.

[17] L. Xiong, Q. Long, Y. Wang, Y. Xiang, X. Wu, Z. He, *Ceram. Int.* **2016**, *42*, 14141.
[18] F. Li, Z. Xu, Q. Sun, D. Hong, C.-Y. Xu, Y. Wang, H.-T. Fang, *ACS Appl. Mater. Interfaces* **2019**, *11*, 35667.
[19] C. Gao, H. Liu, S. Bi, S. Fan, X. Meng, Q. Li, C. Luo, *J. Materiomics* **2020**, *6*, 712.
[20] C. Gao, H. Liu, S. Bi, S. Fan, Q. Liu, H. Li, L. Cao, C. Luo, *J. Phys. Chem. C* **2020**, *124*, 18847.
[21] H. Chen, P. He, M. Li, Y. Wen, G. Cao, J. Qiu, H. Ming, P. Zhao, S. Zhang, *ACS Appl. Energy Mater.* **2021**, *4*, 5963.
[22] Y.-D. Tsai, J.-Y. Shih, Y.-J. J. Li, T.-F. Hung, L.-F. Hsu, S. K. Ramaraj, R. Jose, C. Karuppiah, C.-C. Yang, *ACS Sustainable Chem. Eng.* **2022**, *10*, 16709.
[23] P. S. Kumar, A. Sakunthala, M. Prabu, M. V. Reddy, R. Joshi, *Solid State Ionics* **2014**, *267*, 1.
[24] T. Chi, X. Wang, L. Zeng, Z. Qin, X. Zhou, Z. Liu, *J. Electrochem. Soc.* **2023**, *170*, 040515.
[25] J. Cao, P. He, M. A. Mohammed, X. Zhao, R. J. Young, B. Derby, I. A. Kinloch, R. A. W. Dryfe, *J. Am. Chem. Soc.* **2017**, *139*, 17446.
[26] S. Pei, Q. Wei, K. Huang, H.-M. Cheng, W. Ren, *Nat. Commun.* **2018**, *9*, 145.
[27] V. Nagyte, D. J. Kelly, A. Felten, G. Picardi, Y. Shin, A. Alieva, R. E. Worsley, K. Parvez, S. Dehm, R. Krupke, S. J. Haigh, A. Oikonomou, A. J. Pollard, C. Casiraghi, *Nano Lett.* **2020**, *20*, 3411.
[28] Y. Fu, Q. Wei, G. Zhang, Y. Zhong, N. Moghimian, X. Tong, S. Sun, *Materials* **2019**, *12*, 842.
[29] J. Chen, H. Li, L. Zhang, C. Du, T. Fang, J. Hu, *Sci. Rep.* **2020**, *10*, 3124.
[30] K. H. Park, D. W. Kang, J.-W. Park, J.-H. Choi, S.-J. Hong, S. H. Song, S.-M. Lee, J. Moon, B. G. Kim, *J. Mater. Chem. A* **2021**, *9*, 1822.
[31] X. Fan, C. Wang, *Chem. Soc. Rev.* **2021**, *50*, 10486.
[32] S. Masubuchi, T. Machida, *npj 2D Mater. Appl.* **2019**, *3*, 4.
[33] D. Nečas, P. Klapetek, *Open Phys.* **2012**, *10*, 181.
[34] C. F. Elkjær, L. F. Høj, *J. Højberg*n.d

Manuscript received: May 9, 2025
Revised manuscript received: September 25, 2025
Version of record online: